

Article

Equivalent Method of Joint Interface Based on Persson Contact Theory: Virtual Material Method

Renxiu Han ^{1,*}, Guoxi Li ¹, Jingzhong Gong ², Meng Zhang ¹ and Kai Zhang ¹ 

¹ College of Mechatronics Engineering and Automation, National University of Defense Technology, No.109 Deya Street, Changsha 410073, China; lgx2020@sina.com (G.L.); zhangmengchn@126.com (M.Z.); kai277063148@163.com (K.Z.)

² School of Mechanical Engineering, Hunan International Economics University, No.822 Fenglin Street, Changsha 410205, China; jzgong@nudt.edu.cn

* Correspondence: hanrenxiu17@nudt.edu.cn; Tel.: +86-1327-204-8693

Received: 13 September 2019; Accepted: 25 September 2019; Published: 26 September 2019



Abstract: An accurate equivalent method of metal joint interface is of great significance to optimize the dynamic performance of the whole machine. Therefore, it is necessary to establish an accurate equivalent method of joint interface. The virtual material method is a precise equivalent method of joint interface. The traditional virtual material method is based on the M–B fractal contact theory. By modeling the contact mechanics of the joint interface, the physical properties of the virtual material are obtained separately, such as elastic modulus, Poisson’s ratio and density. In this paper, Persson contact theory is used to establish the interface contact mechanics model to find the physical properties of virtual materials. The virtual material methods constructed by two theories are respectively applied to the modal simulation to obtain the natural frequencies of the joint interface. By comparing the natural frequencies obtained by modal experiment and modal simulation, it is found that the natural frequencies obtained by the virtual material method based on Persson contact theory are closer to the results obtained by the modal experiment, and the error is within 5%. The error of the natural frequencies obtained by the virtual material method based on the M–B fractal contact theory is within 10%. Therefore, the Persson contact theory can establish a more accurate equivalent method of metal’s joint interface.

Keywords: equivalent method of interface; Persson contact theory; virtual material method

1. Introduction

The part connecting the upper and lower surfaces between the components is called the mechanical joint interface, which is ubiquitous in the mechanical structure. Through the study of the joint interface, the scholars found that the 50% total stiffness, and more than 90% total damping of the machine tool comes from the joint interface [1]. Therefore, the establishment of an accurate equivalent method of joint interface is of great significance for engineering applications. According to the recent studies [2–6], the equivalent method of joint interface includes a virtual material method, spring damping method, and finite element method. By comparing the mode shapes and the natural frequencies obtained by modal experiment and modal simulation [5], it is found that the virtual material method can better simulate the metal joint interface than the other two methods.

A large number of studies have shown that [7–10] most of the machined surfaces have statistical self-affine characteristics. The rough surface similarity is unique at different scales. Even at the atomic scale, the surface morphology still has multi-scale, self-affine and non-stationary features, namely fractal characteristics. The function simulates a rough surface with good agreement with the measured surface. Its fractal roughness parameter G , fractal dimension D and Hurst exponent H are dimension independent. Therefore, the fractal theory can reflect the actual surface contour of the assembly

joint interface more realistically and reliably. In addition, many scholars [11–14] study the relevant characteristics of the joint interface through fractal theory, and explain the importance of fractal theory to the research of the joint interface.

The virtual material method was proposed by Tian Hongliang [2]. This method uses the M–B fractal contact theory [15,16] to establish the contact mechanics model of the mechanical joint interface, and obtains the physical parameters of the virtual material from the microscopic point of view, such as Poisson’s ratio, density, elastic modulus, etc. Through the comparison of experiments and simulations [2,5], it is found that the error of the virtual material method established by the M–B fractal contact theory is large, which is about 10%. However, the M–B contact mechanics model has certain limitations. The contact mechanics model ignores the interaction between the asperities. When the pressing force is small, this assumption is approximately true, but when the pressing force is relatively large, the interaction between the asperities cannot be ignored. Therefore, it will affect the establishment of the equivalent model. In recent years, Persson et al. used mathematical methods such as fractal geometry and frequency domain transformation to draw a set of contact mechanics theory considering scale effect [17–27]. The mechanics model considers the effect of scale effects on contact behavior and the interaction between asperities. In order to consider the effect of the surface roughness scale effect on the contact behavior, the model assumes that the deformation of the surface asperities or dimples is approximately equal to the height of the surface asperities or the depth of the dimples. This assumption applies only to situations where the pressing force (actual contact area) is large, but it does not apply to situations where the pressing force (actual contact area) is relatively small. This boundary condition is suitable for the metal joint interface studied in this paper. Through experimental and theoretical calculations [26], it is found that, with the increase in pressure, the theoretically calculated stiffness between the joint interface can be well fitted to the actual stiffness between the joint interface.

Constructing an accurate equivalent method of joint interface can accurately analyze the dynamic performance of the whole machine. In this paper, two different joint interface contact mechanics theories are used to construct the equivalent model of the joint interface, namely the virtual material method. Through the comparative analysis of modal experiment and modal simulation, a better theoretical method for constructing the equivalent model of the joint interface is obtained.

2. Materials and Methods

The specimens, made of the same material (GB: 45#, JIS: S45C, ANSI: 1045, DIN:C45), had $L = 0.2$ m length, $l = 0.06$ m thickness. The specimens were pressed by the pressure 0.125 MPa by six bolts, as shown in Figure 1. The specimens are machined by milling and have a surface roughness of approximately $3.2 \mu\text{m}$. The physical properties of the specimens are shown in Table 1. Considering that the joint interface of the machine is usually composed of the same material, the specimens of the same material are selected.

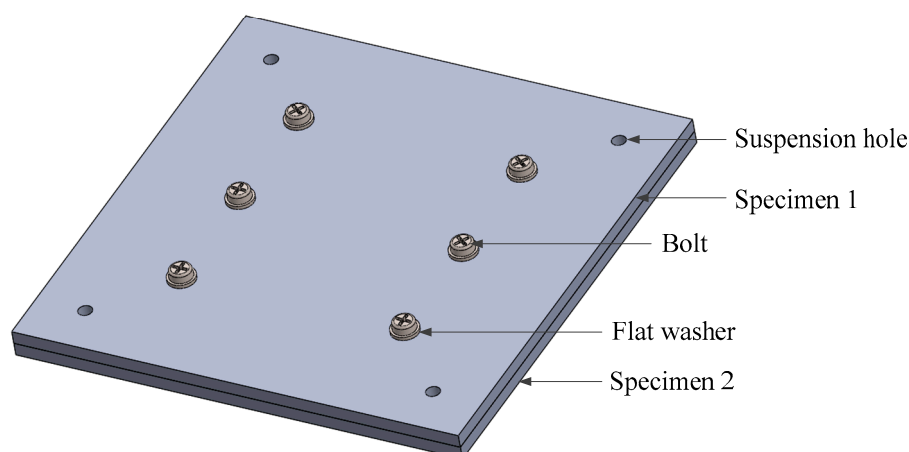


Figure 1. Schematic diagram of the experimental specimens.

Table 1. Physical properties of specimens.

Parameter	Specimens
Elastic modulus: E (GPa)	209
Poisson's ratio: μ	0.3
Density: ρ (kg/m ³)	7850
Roughness: Ra (μm)	3.2
Yield strength: σ_y (MPa)	355
Hardness: H (MPa)	190

The microscopic contact portion of the two contact surfaces of the fixed joint interface is assumed to be a virtual isotropic material as described in Ref. [2]. The length and width of the virtual material are the length and width of the specimens, respectively. The elastic modulus, Poisson's ratio, and density of the virtual material are obtained by some theoretical methods and the thickness of the virtual material is determined according to the actual gap between the two surfaces, which is the virtual material method. In the following, the virtual materials are constructed by Persson contact theory and M-B fractal contact theory, respectively, so as to find a better theoretical method for constructing the equivalent model of joint interface.

2.1. Virtual Material Method Based on Persson Contact Theory

2.1.1. The Surface Roughness Power Spectrum

The data of specimens' surfaces height are acquired by a coordinate measuring machine (ACCURA II AKTIV; Carl Zeiss AG, Oberkochen, Germany, as shown in Figure 2a. The sampling interval of the data is $a = 0.001$ m. Experiment takes 200×200 data points of surface height. The data are fitted to the surface of the specimens by software (MATLAB 2014; MathWorks, Inc., Natick, MA, USA), as shown in Figure 2b.

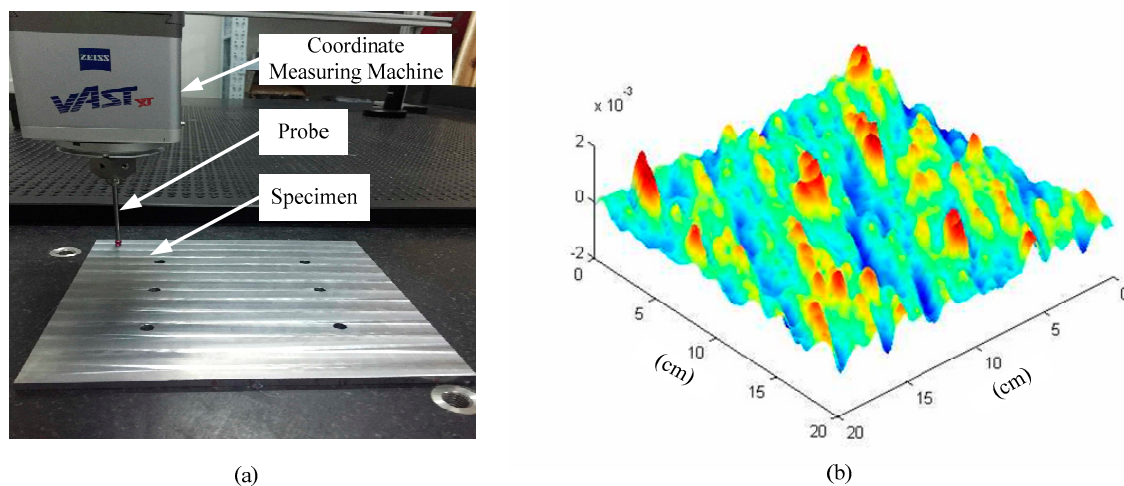


Figure 2. (a) acquisition of surface height data, and (b) a computer-generated rough substrate.

According to the authors in [27], the surface roughness power spectrum $C(q)$ can be written as:

$$C(q) = \frac{(2\pi)^2}{A} \langle |h_A(q)|^2 \rangle, \quad (1)$$

where A is the surface area, $h_A(q)$ is the Fourier transform of the surface height $h(x)$, which can be written as:

$$h_A(q) \approx \frac{a^2}{(2\pi)^2} \sum_n h_n(X_n) e^{-i(2\pi m_x n_x a + 2\pi m_y n_y a)/L}, \tag{2}$$

where a is the length of the specimen, and $n_x = 1, 2, \dots, 200$, $n_y = 1, 2, \dots, 200$, m_x and m_y are integers between 0–199.

Mean square roughness amplitude can be obtained from the acquired data of the surface height:

$$h_{rms}^2 = \langle h^2 \rangle = \frac{1}{N^2} \sum_n (h_n - \bar{h})^2, \tag{3}$$

where $N = 200$, \bar{h} is the average of the surface height, $\langle \dots \rangle$ indicates statistical average of the physical quantities in angle brackets.

Substituting the values of the surface profile height into Equations (1) and (2), the surface roughness power spectrum can be obtained, as shown in Figure 3, where $q_r = 2\pi/L$ is characteristic frequency, $q_0 = 2\pi/\lambda_0$ is minimum cut-off frequency, $q_1 = 2\pi/\lambda_1$ is maximum cut-off frequency, λ_0 is long-wavelength roll-off and λ_1 is short wavelength cut-off.

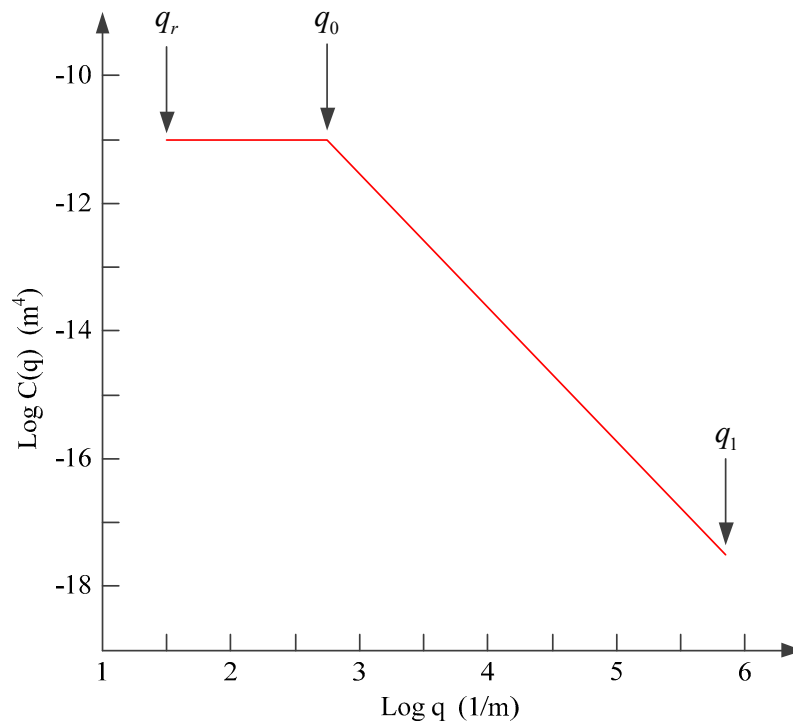


Figure 3. The surface roughness power spectrum.

2.1.2. The Normal Stiffness Model of Interface

According to the authors in [26], the dimensionless elastic energy stored in the Hertz mesoscale deformation field for depth of indentation is written as:

$$U'_0 = \frac{4}{3} \kappa_0 \chi^{-1/(1+H)} \left(\frac{3F'}{4} \right)^{(1+2H)/(1+H)}, \tag{4}$$

where $\kappa_0 = 2/5$ is the root-mean-square curvature of the surface, F' is the dimensionless normal force, $H = 3 - D$ is the Hurst exponent, and χ is the dimensionless prefactor which is obtained by:

$$\chi = \left(\frac{2-H}{Hs_0} \right)^{1/2} \frac{\pi^{H-2}}{\beta q_0 h_{rms}}, \tag{5}$$

where $\beta = \sqrt{8/3\pi}$ when $q_1/q_r \gg 1$, $1/s_0 = 1 + H[1 - (q_r/q_0)^2]$.

The dimensionless elastic deformation energy [25] that is stored in microasperity contacts within the Hertz mesoasperity contact region is obtained by:

$$U'_1 = \frac{4}{3} \kappa_1 \chi^{-1/(1+H)} \left(\frac{3F'}{4} \right)^{(1+2H)/(1+H)}, \tag{6}$$

where $\kappa_1 = \gamma \left(\frac{2-H}{\pi^4 \beta^2 H} \right)^{1/2}$ is the prefactor, $\gamma \approx 0.4$ according to Ref. [26].

The total dimensionless elastic energy is now given by the sum of the two contributions Equations (4) and (6):

$$U' = \frac{4}{3} \kappa \chi^{-1/(1+H)} \left(\frac{3F'}{4} \right)^{(1+2H)/(1+H)}, \tag{7}$$

$$\kappa = \kappa_0 + \kappa_1. \tag{8}$$

The total dimensionless stiffness of the interface is written as:

$$k' = \frac{F'}{dU'/dF'} = \theta \left(\frac{F'}{q_0 h_{rms} s^{1/2}} \right)^{1/(1+H)}. \tag{9}$$

Dimensionless to Equation (9) is written as:

$$\frac{Kh_{rms}}{E^*} = \theta \left(\frac{h_{rms}}{2\pi\lambda_r} \frac{\lambda_r^2}{L^2} \right)^{H/(1+H)} \left(\frac{p}{s^{1/2}E^*} \right)^{1/(1+H)}, \tag{10}$$

where θ is the prefactor that is obtained by Ref. [26], $p = F/A_0$ is the surface pressure, and E^* is the equivalent elastic modulus.

The elastic modulus E and the shear modulus G_τ of the interface can be written as [28]:

$$E = hKn/A_0, \tag{11}$$

$$G_\tau = K_\tau h/A_0, \tag{12}$$

where K_τ is the tangential contact stiffness, and $h = 0.8$ is the thickness of the virtual material according to Ref. [2]. The ratio of the tangential contact stiffness to the normal contact stiffness is 0.25–0.35. Without loss of generality, K_τ/K_n is taken as 0.35, according to Ref. [29].

The Poisson's ratio and density of the virtual material can be described as [4,30] respectively:

$$v = \frac{E}{2G_\tau} - 1, \tag{13}$$

$$\rho = \frac{\rho_1 h_1 + \rho_2 h_2}{h_1 + h_2}, \tag{14}$$

where ρ_1, ρ_2 and h_1, h_2 are the density and thickness of specimen1 and specimen2, respectively.

The physical properties of the virtual material obtained by Equations (10)–(14) are as follows: $E_1 = 0.0591$ Gpa, $\nu_1 = 0.429$, $\rho_1 = 7850$ kg/m³ and $h_1 = 0.8$ mm.

2.2. Virtual Material Method Based on M–B Fractal Contact Theory

The shape of the rough microcontacts on the actual surface is usually an ellipsoid. Since the contact area of the ellipsoid is much smaller than the radius of the curvature of itself, the microcontact can be approximated as a sphere. The contact between the two planes can be seen as a series of bumps in contact with each other. The contact of the two sphere microcontacts is shown in Figure 4.

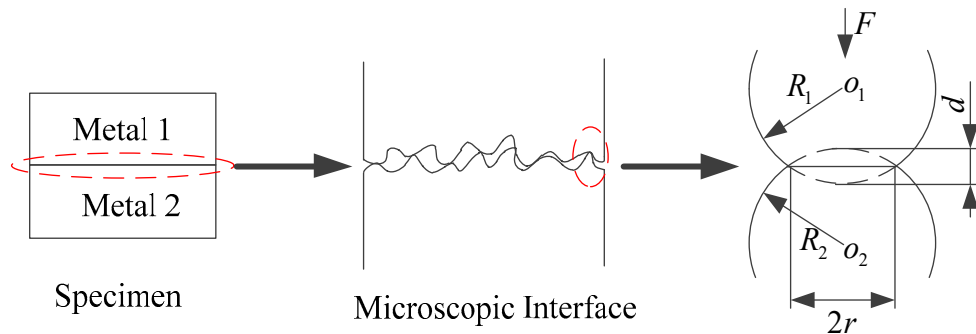


Figure 4. Contact deformation of macroscopic metal joint interface to microscopic contact point.

According to the authors in [31], the normal load of an elastic microcontact is obtained from the hemispherical positive stress of hemisphere:

$$F = \frac{4}{3}E^* \sqrt{R_0d^3}, \tag{15}$$

where R_0, d, E^* are the equivalent curvature radius of the two contacting microcontacts, the deformation of contact point as shown in Figure 4, and the equivalent elastic modulus of the two contact rough surfaces, respectively:

$$R_0 = \frac{R_1 \times R_2}{R_1 + R_2}, \tag{16}$$

$$d = G^{D-1}a'^{1-0.5D}, \tag{17}$$

$$\frac{1}{E^*} = \frac{1-\mu_1^2}{E_1} + \frac{1-\mu_2^2}{E_2}, \tag{18}$$

where μ_1, μ_2 and E_1, E_2 are Poisson’s ratio and elastic modulus of two objects that constitute the joint interface; $a = a'/2 = \pi R_0d$ is the area of a micro contact point. G and D are fractal parameters. According to the authors in [2], fractal parameters are determined by the roughness of the surface of the joint interface. When the metal surface roughness ranges from 0.4 μm to 3.2 μm , the values of G and D are more accurate.

From Equation (15), the actual normal contact compressive stress of an elastic microcontact is written as:

$$P = \frac{F}{\pi r^2} = \frac{F}{a} = \frac{4E^*}{3\pi} \sqrt{\frac{d}{R_0}} = \frac{4E^* \sqrt{\varepsilon}}{3\pi}, \tag{19}$$

where $\varepsilon = d/R_0$ is the normal compressive strain of an elastic micro-contact point.

Differentiating Equation (19), the elastic modulus of two contacting microcontacts is expressed as:

$$e = \frac{dP}{d\varepsilon} = \sqrt{\frac{2}{9\pi^3}} E^* G^{1-D} a'^{0.5D-0.5}. \tag{20}$$

The statistical distribution of the truncated micro-contact area a' can be described as [31]:

$$n(a') = 0.5D\psi^{1-D/2} a_1^{0.5D} a'^{-1-0.5D} \quad (0 < a' \leq a_1), \tag{21}$$

where ψ describes the domain extension factor for the micro-contact size distribution associated with D :

$$a'_1 = 2a_1 = \frac{2(2-D)}{D} \psi^{0.5D-1} A_r, \tag{22}$$

$$a'_2 = 2a_2 = 2G^2 \left(\frac{2E^*}{H} \right)^{\frac{2}{D-1}}, \tag{23}$$

where a_1 is the truncated area of the largest elastic micro-contact, a_2 is the critical truncated area demarcating the elastic and plastic deformation regimes, A_r is actual contact area and H is the hardness of material.

The equivalent elastic modulus can be obtained as:

$$E = \frac{\int_{a'_2}^{a'_1} en(a')ada'}{A_0} = \frac{2^{(2D-9)/2} E^* D \psi^{1-D/2} G^{1-D} a'^{D/2} (a_1^{0.5} - a_2^{0.5})}{3\pi^{(1+D)/2} (\ln \gamma)^{1/2} A_0} \quad (a'_1 < a' < a'_2), \tag{24}$$

where γ is the scaling parameter, and A_0 is nominal contact area.

The physical properties of the virtual material obtained by Equations (11)–(24) are as follows: $E_2 = 0.1253$ Gpa, $\nu_2 = 0.429$, $\rho_2 = 7850$ kg/m³ and $h_2 = 0.8$ mm.

3. Modal Simulation, Modal Experiment and Results

3.1. Modal Simulation

The virtual material method is modeled in three dimensions through software (SOLIDWORKS 2018; Dassault Systemes, Waltham, MA, USA). The model is imported into software (ANSYS Workbench 14.0; ANSYS, Inc., Pittsburgh, PA, USA). The physical parameters listed in Table 1 are assigned to specimen1 and specimen2. The physical parameters obtained by Persson contact theory and M–B fractal contact theory are respectively assigned to virtual materials. The mesh diagram of the model is shown in Figure 5. The grid has a total of 140,517 nodes and 75,588 elements. The pressing force of 0.125MPa is applied to the specimens as the boundary condition. Finally, the modal analysis is performed to obtain the first five natural frequencies of the specimens, as shown in Table 2.

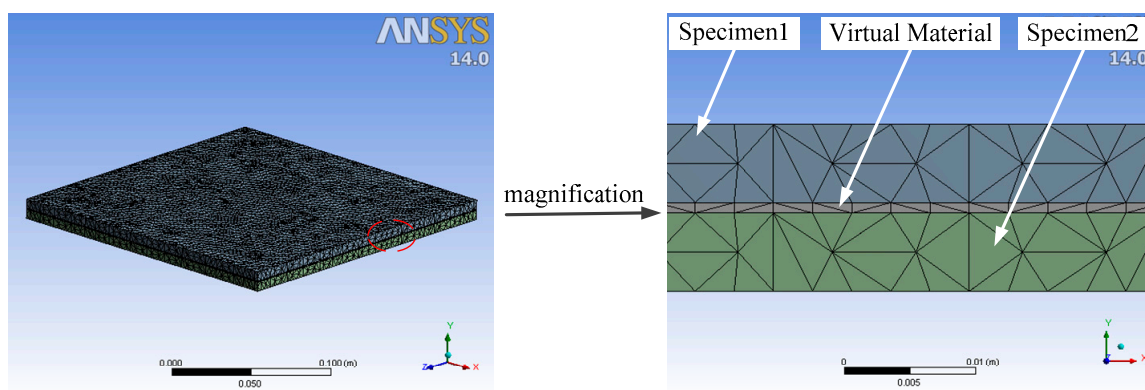


Figure 5. Grid diagram of the virtual material method.

Table 2. The first five natural frequencies of the model obtained from modal simulation.

Frequency	f_1 (Hz)	f_2 (Hz)	f_3 (Hz)	f_4 (Hz)	f_5 (Hz)
Persson contact theory	720.4	1141.3	1355.0	1524.1	1635.1
M–B contact theory	745.5	1201.8	1403.8	1600.1	1725.2

3.2. Modal Experiment

The experimental setup (PSV-I-500; Polytec GmbH, Waldbronn, Germany) is as shown in Figure 6a. The experimental specimens are suspended by two elastic ropes in front of the exciter to reach the boundaryless condition and excited by an exciter. Experimental data are acquired by laser scanning specimens. Finally, the processing of the data is shown in Figure 6b. The first five natural frequencies of the specimens are shown in Table 3.

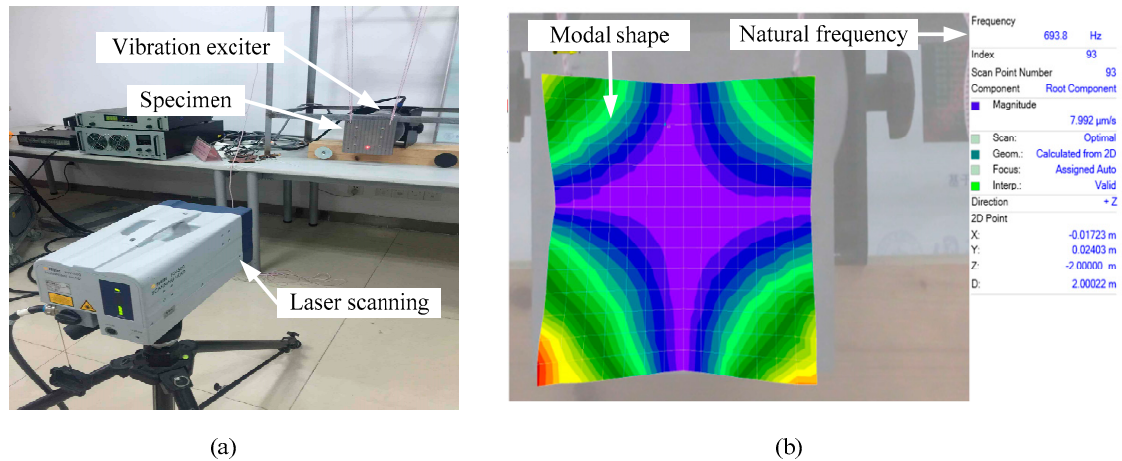


Figure 6. (a) experimental setup, and (b) modal analysis of the first order by computer.

Table 3. The first five natural frequencies of the model obtained from the modal experiment.

Frequency	f_1 (Hz)	f_2 (Hz)	f_3 (Hz)	f_4 (Hz)	f_5 (Hz)
Modal experiment	693.8	1093.8	1292.2	1459.4	1567.2

3.3. Results

The first five natural frequencies and errors obtained from modal experiment and modal simulation are shown in Table 4. By comparison analysis, the error of the first five natural frequencies obtained by the virtual material method based on Persson contact theory is within 5%. The error of the virtual material method based on the M–B fractal contact theory is within 10%.

Table 4. The errors of the first five natural frequencies obtained from modal experiment and modal simulation.

Order	1	2	3	4	5
Error of Persson	3.78%	4.34%	4.86%	4.43%	4.34%
Error of M–B	7.45%	9.87%	8.57%	9.63%	10.0%

4. Conclusions

According to the authors in [5], the first five modal shapes obtained by the virtual material method are consistent with those obtained by the experiment. In addition, it is found that the virtual material method can better simulate the metal joint interface than the spring damping method and the finite element method. Therefore, it can be proved that the virtual material method can be equivalent to the metal joint interface. However, the traditional virtual material method is based on fractal contact theory and has certain limitations. The contact mechanics model ignores the interaction between the asperities. When the pressing force (actual contact area) is small, this assumption is approximately true, but when the pressing force (actual contact area) is relatively large, the interaction between the asperities cannot be ignored. Therefore, it will affect the establishment of the equivalent model. In

this paper, the Persson contact theory is used to compute the physical properties of virtual materials. The Persson contact theory takes into account the interaction between the asperities. In addition, when the pressing force (actual contact area) of the joint interface is larger, the more accurate the result is, which is suitable for the mechanical joint interface. According to the results of modal experiment and modal simulations, the fact that the error of the first five natural frequencies obtained by the virtual material method and the modal experiment based on Persson contact theory is within 5%, compared with the 10% error of the traditional virtual material method, is a great improvement. Therefore, the physical parameters of virtual materials obtained by Persson contact theory are more accurate, which is more suitable for establishing the virtual material method, so as to achieve accurate analysis of the performance of the whole machine.

Author Contributions: The modal experiment was completed by R.H. and K.Z. under the supervision of G.L., J.G. and M.Z. The simulation was completed by R.H. under the guidance of G.L. and M.Z. R.H. wrote the paper.

Funding: This research was funded by the National Natural Science Foundation of China, Grant No. 51775552 and the Key Research Project of the Education Department of Hunan Province, Grant No. 15A107.

Conflicts of Interest: The authors declare no conflict of interest.

References

1. Ibrahim, R.A.; Pettit, C.L. Uncertainties and dynamic problems of bolted joints and other fasteners. *J. Sound Vib.* **2005**, *279*, 857–936. [[CrossRef](#)]
2. Tian, H.; Li, B.; Liu, H.; Mao, K.; Peng, F.; Huang, X. A new method of virtual material hypothesis-based dynamic modeling on fixed joint interface in machine tools. *Int. J. Mach. Tool Manuf.* **2011**, *51*, 239–249. [[CrossRef](#)]
3. Huang, K.; Jin, J. Research on bolt preload simulation based on virtual material method. *Mach. Des. Manuf.* **2012**, *8*, 148–150.
4. Zhao, Y.; Yang, C.; Cai, L.; Shi, W.; Liu, Z. Surface contact stress-based nonlinear virtual material method for dynamic analysis of bolted joint of machine tool. *Precis. Eng.* **2016**, *43*, 230–240. [[CrossRef](#)]
5. Han, R.; Li, G.; Gong, J.; Zhang, M.; Zhang, K. Experimental verification and comparative analysis of equivalent methods on metal's fixed joint interface. *Materials* **2019**, *12*, 2381. [[CrossRef](#)] [[PubMed](#)]
6. Jana, T.; Anirban, M.; Prasanta, S. Dynamic contact interactions of fractal surfaces. *Appl. Surf. Sci.* **2017**, *392*, 872–882. [[CrossRef](#)]
7. Majumdar, A.; Tien, C.L. Fractal characterization and simulation of rough surfaces. *Wear* **1990**, *136*, 313–327. [[CrossRef](#)]
8. Gagnepin, J.J.; Roques-Carmes, C. Fractal approach to two-dimensional and three-dimensional surface roughness. *Wear* **1990**, *109*, 114–119. [[CrossRef](#)]
9. Lopez, J.; Hansali, G.; Zahouani, H. 3D fractal-based characterization for engineered surface topography. *Int. J. Mach. Tools Manuf.* **1995**, *35*, 211–217. [[CrossRef](#)]
10. Marotta, E.E.; Fletcher, L.S.; Dietz, T.A. Thermal contact resistance modeling of non-flat, roughened surfaces with non-metallic coatings. *J. Heat Transf.* **2001**, *123*, 11–23. [[CrossRef](#)]
11. Panagouli, O.K.; Mastrodimitou, K. Dependence of friction coefficient on the resolution of asperities in metallic rough surfaces under cyclic loading. *Int. J. Solids Struct.* **2017**, *108*, 85–97. [[CrossRef](#)]
12. Panagouli, O.K.; Iordanidou, K. Dependence of friction coefficient on the resolution and fractal dimension of metallic fracture surfaces. *Int. J. Solids Struct.* **2013**, *50*, 3106–3118. [[CrossRef](#)]
13. Panagouli, O.K.; Mistakidis, E. Dependence of contact area on the resolution of fractal interfaces in elastic and inelastic problems. *Eng. Comput.* **2011**, *28*, 717–746. [[CrossRef](#)]
14. Panagiotopoulos, P.D.; Mistakidis, E.S.; Panagouli, O.K. Fractal interfaces with unilateral contact and friction conditions. *Comput. Method Appl. Mech. Eng.* **1992**, *99*, 395–412. [[CrossRef](#)]
15. Yuan, Y.; Gan, L.; Liu, K.; Yang, X. Elastoplastic contact mechanics model of rough surface based on fractal theory. *Chin. J. Mech. Eng.* **2017**, *30*, 207–215. [[CrossRef](#)]
16. Majumdar, A.; Bhushan, B. Role of fractal geometry in roughness characterization and contact mechanics of surfaces. *J. Tribol.* **1990**, *112*, 205–216. [[CrossRef](#)]
17. Persson, B.N.J. On the fractal dimension of rough surfaces. *Tribol. Lett.* **2014**, *54*, 99–106. [[CrossRef](#)]

18. Persson, B.N.J. Theory of rubber friction and contact mechanics. *J. Chem. Phys.* **2001**, *115*, 3840–3861. [[CrossRef](#)]
19. Yang, C.; Persson, B.N.J. Molecular dynamics study of contact mechanics: Contact area and interfacial separation from small to full contact. *Phys. Rev. Lett.* **2008**, *100*, 024303. [[CrossRef](#)]
20. Yang, C.; Persson, B.N.J. Contact mechanics: Contact area and interfacial separation from small contact to full contact. *J. Phys.* **2008**, *20*, 215214. [[CrossRef](#)]
21. Persson, B.N.J. On the elastic energy and stress correlation in the contact between elastic solids with randomly rough surfaces. *J. Phys.* **2008**, *20*, 312001. [[CrossRef](#)]
22. Almqvist, A.; Campana, C.; Prodanov, N.; Persson, B.N.J. Interfacial separation between elastic solids with randomly rough surfaces: Comparison between theory and numerical techniques. *J. Mech. Phys. Solids* **2011**, *59*, 2355–2369. [[CrossRef](#)]
23. Persson, B.N.J. Contact mechanics for randomly rough surfaces. *Surf. Sci. Rep.* **2006**, *61*, 201–227. [[CrossRef](#)]
24. Persson, B.N.J.; Bucher, F.; Chiaia, B. Elastic contact between randomly rough surfaces: Comparison of theory with numerical results. *Phys. Rev.* **2002**, *65*, 184106. [[CrossRef](#)]
25. Persson, B.N.J. Relation between interfacial separation and load: A general theory of contact mechanics. *Phys. Rev. Lett.* **2007**, *99*, 125502. [[CrossRef](#)] [[PubMed](#)]
26. Pastewka, L.; Prodanov, N.; Lorenz, B.; Müser, M.H.; Robbins, M.O.; Persson, B.N.J. Finite-size scaling in the interfacial stiffness of rough elastic contacts. *Phys. Rev.* **2013**, *87*, 062809. [[CrossRef](#)] [[PubMed](#)]
27. Persson, B.N.J.; Albohr, O.; Tartaglino, U.; Volokitin, A.I.; Tosatti, E. On the nature of surface roughness with application to contact mechanics, sealing, rubber friction and adhesion. *J. Phys.-Condens. Matter* **2005**, *17*, R1–R62. [[CrossRef](#)] [[PubMed](#)]
28. Pan, W.; Li, X.; Wang, L.; Guo, N.; Mu, J. A normal contact stiffness fractal prediction model of dry-friction rough surface and experimental verification. *Eur. J. Mech. Solid* **2017**, *66*, 94–102. [[CrossRef](#)]
29. Mayer, M.H.; Gaul, L. Segment-to-segment contact elements for modelling joint interfaces in finite element analysis. *Mech. Syst. Signal Proc.* **2007**, *21*, 724–734. [[CrossRef](#)]
30. Ye, H.; Huang, Y.; Li, P.; Li, Y.; Bai, L. Virtual material parameter acquisition based on the basic characteristics of the bolt joint interfaces. *Tribol. Int.* **2016**, *95*, 109–117. [[CrossRef](#)]
31. Wang, S.; Komvopoulos, K. A fractal theory of the interfacial temperature distribution in the slow sliding regime: Part I—Elastic contact and heat transfer analysis. *J. Tribol.* **1994**, *116*, 812–823. [[CrossRef](#)]



© 2019 by the authors. Licensee MDPI, Basel, Switzerland. This article is an open access article distributed under the terms and conditions of the Creative Commons Attribution (CC BY) license (<http://creativecommons.org/licenses/by/4.0/>).